Microscopic spin-distortion model for switchable molecular solids: Spatiotemporal study of the deformation field and local stress at the thermal spin transition

Ahmed Slimani, Kamel Boukheddaden,* François Varret, and Hassane Oubouchou
Groupe d'Etudes de la Matière Condensée, Université de Versailles–CNRS UMR 8635, 45 Avenue des Etats Unis, 78035 Versailles Cedex, France

Masamichi Nishino
Computational Materials Science Center, National Institute for Materials Science, Tsukuba, Ibaraki 305-0047, Japan

Seiji Miyashita
Department of Physics, Graduate School of Science, The University of Tokyo, Bunkyo-Ku, Tokyo and CREST, JST, 4-1-8 Honcho Kawaguchi, Saitama 332-0012, Japan

(Received 2 April 2012; revised manuscript received 19 September 2012; published 22 January 2013)

We design a microscopic model for switchable molecular solids (e.g., spin crossover), based on the elastic properties of a discrete lattice made of switchable sites, denoted high spin (HS) or low spin (LS). The elastic interactions and equilibrium distances between sites are written as explicit functions of their HS or LS states. The model was solved by Monte Carlo technique, alternatively running on the electronic and position variables. In the present work we investigate the thermal transition in the case of a square two-dimensionsal lattice, including short-range interactions up to the second neighbors in order to maintain the stability of the lattice. The input values of the elastic parameters are selected so as to lead to realistic values of the bulk modulus and Debye temperature. We show that the elastic interactions act as effective Ising interactions, leading to the expected transition and phase diagram, in terms of transition temperature vs elastic interaction parameter. We study the domain growth of the LS or HS species at different temperatures along the thermal loop and obtain features consistent with the experimental data. We also follow the mechanical properties of the system by calculating the displacement field and the internal stresses produced by the domain growth process. The resulting maps evidence the leading role of the HS/LS interface and the crucial effect of the edges of the lattice, thus paving the way to a real understanding of the shape effects in spin transition nanocrystals.

DOI: 10.1103/PhysRevB.87.014111 PACS number(s): 62.20.−x, 75.30.Wx, 75.50.Xx, 75.78.Fg

I. INTRODUCTION

The thermally induced spin crossover (SC) transition between the low-spin (LS) and the high-spin (HS) states of Fe(II) complexes with suitable ligands is a typical example of switchable molecular solids (SMCs). SMCs have been studied[1–3] for many years due to their promising applications as materials for information storage. The bistability of SMCs originates from an intramolecular vibronic coupling[4] and can be enhanced at the solid state by intermolecular interactions. Indeed, elastic interactions[5–7] are recognized as a basic ingredient of the SC transition and lead to various behaviors: from gradual, with a transition corresponding to the simple Boltzmann distribution between two states which is generally obtained in highly diluted crystals (i.e., in noncooperative systems), to rather abrupt thermal spin transitions, and even up to hysteretic behavior denoting a first-order phase transition[8–10] above a threshold value of the interaction strength. The occurrence of two-step transitions has been assigned to the coexistence of interactions with opposite signs.[10,11] Most of the models developed historically (regular solutions,[12] Ising-like[13,14]) are based on two-level approaches which totally discard the volume change at the transition and, consequently, the effect of mechanical stresses on the transition mechanism. In such models, the first-order thermal transition is obtained through a phenomenological interaction parameter, electronic in nature. At variance from these electronic models, the continuous medium model developed by H. Spiering[6] showed that an elastic interaction could also give rise to the observed first-order transitions. More recently, discrete models based on deformable lattices[15–21] were introduced so as to mimic the spatiotemporal features of the nucleation and growth (NG) process of spin phases, which were revealed by optical microscopy investigations[22–24] at the thermal transition of SC single crystals. The present work aims to conciliate the continuous medium and discrete lattice approaches with purely elastic interactions, so as to reproduce both the lattice and the spin transformations of the system, thus giving access to spatiotemporal properties. The relevance of the model is established through its ability to reproduce, at least qualitatively, the spatiotemporal effects reported as follows in the well-documented case of the HS → LS transition of fresh single crystals: (i) the transition usually starts from a corner and/or an edge of the crystal (depending on its shape); (ii) the LS phase spreads over the whole crystal with a well-defined frontline, the shape of which depends on the interplay with the edges of the crystal; (iii) the frontline propagates at a very slow velocity (≈2–10 μm/s); (iv) the existence of large mechanical stresses is evidenced by irreversible damage; and (v) the stresses (after thermal cycling) strongly impact the subsequent transition temperatures. By proceeding to a local analysis of the kinetics of the transformation, we deduced that the NG process at the thermal transition is a multiscale process driven by the propagation of mechanical stresses ahead

of the transformation frontline.[23] These results pointed out the importance of the coupling between the spin-state change and the local deformation of the lattice, opening the way to very interesting theoretical problems in which electronic (spin) and structural (lattice parameter) degrees of freedom are coupled. The present problem is similar to that of miscibility and superstructure formation in binary solid alloys, which in the past was studied in the frame of lattice-gas statistical models. However, these historical lattice-gas models involve rigid lattices and actually belong to the class of two-level models previously quoted.[12–14] More recent models were proposed on the basis of deformable lattices with various interaction potentials.[15–20] Indeed, the choices of a proper interaction potential and of the degrees of freedom of the sites are crucial issues. Long-range potentials may be very time-consuming. Therefore, we use here a short-range anharmonic quartic potential, recently introduced and exactly solved for the one-dimensional (1D) case by the transfer integral method.[25] The present work is restricted to the case of a 2D square lattice, with fixed topology. It is solved by a Monte Carlo algorithm which alternatively changes the spin states and moves the nodes in the framework of a canonical ensemble. In the choice of input parameters we aimed to match the experimental values of relevant parameters such as the bulk modulus and Debye temperatures, as well as the structure variations at the transition.

The paper is organized as follows: in Sec. II the model and simulation method are described; in Sec. III the interaction parameter values are derived from the available literature on elastic properties of SC solids; Sec. IV is devoted to the results of the model (phase diagram, spatiotemporal properties of the thermal transition), with a focus on the atomic displacements and the propagation of mechanical stresses; and in Sec. V we summarize the main conclusions and outline some possible developments of the work.

II. THE MODEL: THEORETICAL BACKGROUND

The model consists of a discrete deformable lattice made of two-level units representing the HS and LS states. The lattice is square planar of size $L \times L$. The electronic state of each unit is described by a fictitious spin $S = +1$ (HS) or -1 (LS), with degeneracy ratio $g^{\mathrm{HS}}/g^{\mathrm{LS}} = g$ and energy gap $E^{\mathrm{HS}} - E^{\mathrm{LS}} = \Delta$. We also assumed that the energy gap of an isolated molecule does not depend on temperature. In a previous work,[26,27] we demonstrated that the present Ising-like system, with $g^{\mathrm{LS}} \neq g^{\mathrm{HS}}$, is isomorphic to a pure two-state Ising system under a temperature-dependent field, $-\frac{1}{2}k_B T \ln(g)$. We then obtained an effective temperature-dependent energy gap, $(\Delta - k_B T \ln(g))$, where the second contribution has an entropic origin.

We assumed for simplicity that the lattice deformations remain inside the plane. The molecules at the lattice sites interact by springs between first- and second-nearest neighbors. It is important to mention that the intersite distances used here do not directly refer to the bond lengths between the metal ion and the ligands, which is the distance Fe-N in iron SC materials, for example. The intersite distances actually correspond to the distances between SC metal centers, and the first-neighbor distance is called the lattice parameter or intermolecular distance in the following. The topology of the bond network will be maintained during the simulation, irrespective of the actual values of the lattice parameters. In the present case of a square planar lattice, the presence of second-neighbor interactions is needed to ensure mechanical stability with respect to shear distortion. Simulations were performed on a system with open boundary conditions, so as to reveal surface effects, which are expected to be large in the case of nanosize systems. The simulations do not explicitly involve pressure effects.

In this problem, the equilibrium distances between site i and site j depend on the spin states of these sites and are written as $R_0(S_i, S_j)$ and $R_0^{'}(S_i, S_k)$ for the first- and second-neighbor pairs, respectively. The corresponding bond stiffness constants are denoted $A(r_{ij})$ and $B(r_{ij})$, where r_{ij} is the distance between site i and site j. The electromechanical Hamiltonian is written

$$H = H_{\mathrm{elec}} + H_{\mathrm{elas}}, \tag{1}$$

with H_{elec} a two-state Hamiltonian,

$$H_{\mathrm{elec}} = \sum_i \frac{1}{2}(\Delta - k_B T \ln(g))S_i, \tag{2}$$

and H_{elas} an elastic Hamiltonian,

$$H_{\mathrm{elas}} = \sum_{i-j} \frac{A_{ij}(r_{ij})(r_{ij} - R_0(S_i, S_j))^2}{2} + \sum_{i-k} \frac{B_{ik}(r_{ik})(r_{ik} - R_0^{'}(S_i, S_k))^2}{2}, \tag{3}$$

where

$$A_{ij}(r_{ij}) = A_0 + A_1\left(r_{ij} - R_0^{\mathrm{HH}}\right)^2 \quad \text{and}$$
$$B_{ik}(r_{ik}) = B_0 + B_1\left(r_{ik} - \sqrt{2}R_0^{\mathrm{HH}}\right)^2. \tag{4}$$

Here, $i - j$ and $i - k$, respectively, denote the first- and second-neighbor bonds. The bond vectors and the intermolecular distances are written $\vec{r}_{ij} = \vec{r}_j - \vec{r}_i$ and $\vec{r}_{ik} = \vec{r}_k - \vec{r}_i$, respectively, and $R_0^{\mathrm{HH}} \equiv R_0(1,1)$. The variations of the equilibrium intermolecular distance and bond stiffness result in volume and bulk modulus changes, which are major experimental features of the spin transition leading to an increase in the volume and a decrease in the bulk modulus upon the LS $\rightarrow$ HS transition. Anharmonic contributions, such as those written in Eq. (4) (in terms of even-degree polynomials for ensuring stability of the system with respect to large distortions), can be introduced so as to generate the thermal dependences of the bulk modulus and of the Debye temperature, which can be determined experimentally. We neglected here the third-order contributions to the total elastic constant, which are responsible for the thermal expansion of the lattice. In fact, the anharmonic form of the elastic constant, given in Eq. (4), should be seen as an empirical form, due to the lack of appropriate studies on the elastic constants of SC single crystals, the anisotropy of which makes the Brillouin scattering investigations very complicated.

Let us assume for simplicity that $A_1/A_0 = B_1/B_0$; then the stiffness constant of the lattice only depends on the ratio A_1/A_0. In the present work we took $A_0 = 4 \times 10^3$ K/nm^2, $A_1 \times a^2 = 4 \times 10^4$ K/nm^2, where $a = 1$ nm is the lattice

parameter of the LS state. Namely, $A_{ij}(R_0^{\mathrm{HH}}) = 4 \times 10^3$ K/nm^2 and $A_{ij}(R_0^{\mathrm{LL}}) = 5.6 \times 10^3$ K/nm^2, with $A_0 = B_0$ and $A_1 = B_1$.

The ratio of the elastic constants A_0 and A_1 can be derived from the changes in the Debye temperatures of the HS and LS phases as expressed in Refs. 25 and 28:

$$\frac{\Theta_D^{\mathrm{LL}}}{\Theta_D^{\mathrm{HH}}} = \sqrt{\frac{A\left(R_0^{\mathrm{LL}}\right)}{A\left(R_0^{\mathrm{HH}}\right)}} = \sqrt{1 + \frac{A_1}{A_0}\left(R_0^{\mathrm{LL}} - R_0^{\mathrm{HH}}\right)^2}, \tag{5}$$

where

$$R_0^{\mathrm{LL}} \equiv R_0(-1,-1). \tag{6}$$

As a matter of fact, the anharmonic terms are not needed to obtain the phase transition, and their effect was finally found to be negligible.

Now we turn to a formal transformation of the Hamiltonian, based on an equivalent formulation of the equilibrium distances, as follows:

$$R_0(S_i, S_j) = \rho_0 + \rho_1(S_i + S_j) + \rho_2 S_i S_j. \tag{7}$$

Simple identification to the equilibrium distances for HH, LH, and LL bonds leads to

$$\rho_0 = \tfrac{1}{4}\left(R_0^{\mathrm{HH}} + R_0^{\mathrm{LL}} + 2R_0^{\mathrm{HL}}\right), \quad \rho_1 = \tfrac{1}{4}\left(R_0^{\mathrm{HH}} - R_0^{\mathrm{LL}}\right), \quad \text{and}$$
$$\rho_2 = \tfrac{1}{4}\left(R_0^{\mathrm{HH}} + R_0^{\mathrm{LL}} - 2R_0^{\mathrm{HL}}\right). \tag{8}$$

The parameter ρ_0 is obviously associated with the average lattice parameter of the system, termed a in the following. The parameters ρ_1 and ρ_2 are associated with mismatch of the HS and LS lattices. In the present work we took $\rho_2 = 0$ and consequently termed ρ_1 the *misfit parameter*. In order to derive the analytical dependence of the total potential energy on the stiffness constant and the lattice misfit, we investigated the structure of the Hamiltonian. For making the discussion easier, we only consider in the present section the harmonic part and the nearest-neighbor interactions. Then the total Hamiltonian, (1), is accordingly re-expressed in terms of an Ising-like Hamiltonian with space-dependent effective interactions and effective field:

$$H = \sum_{i-j} J_{ij} S_i S_j + \sum_i h_i S_i + \frac{A_0}{2} \sum_{i-j} (r_{ij} - \rho_0)^2 + C, \tag{9}$$

where the parameters J_{ij} and h_i are the local exchange-like interactions and the local field-like contributions, respectively. The expressions of J_{ij} and h_i are given by

$$J_{ij} = A_0\left[\rho_1^2 - \rho_2(r_{ij} - \rho_0)\right] \tag{10}$$

and

$$h_i = \frac{1}{2}(\Delta - k_B T \ln g) + \frac{z}{2} A_0 \rho_1 \rho_2 - A_0 \rho_1 \sum_{j=1}^{z} (r_{ij} - \rho_0), \tag{11}$$

where the index j runs over the neighbors of a given site i, and z (=4) is the coordination number. The constant C is given by

$$C = \frac{zN}{4} A_0\left(2\rho_1^2 + \rho_2^2\right). \tag{12}$$

The third term in Eq. (9) is related to the cohesion energy of the elastic system, the equilibrium distance of which is given by ρ_0 when the spin variables are absent. The constant term C is omitted hereafter, since it does not play any role in the thermodynamic properties of the system.

In the present simulations, we have used $R_0^{\mathrm{HL}} = \frac{(R_0^{\mathrm{HH}} + R_0^{\mathrm{LL}})}{2}$, and therefore $\rho_2 = 0$, which leads to the following expressions of J_{ij} and h_i:

$$J_{ij} = A_0 \rho_1^2 \tag{13}$$

and

$$h_i = \frac{1}{2}(\Delta - k_B T \ln g) - A_0 \rho_1 \sum_{j=1}^{z} (r_{ij} - \rho_0). \tag{14}$$

Equation (13) clearly shows a spatially invariant effective interaction J_{ij}, which is the product of the elastic constant of the lattice and of the square of the lattice misfit parameter. It also expresses a bilinear coupling between displacements and spins, proportional to ρ_1^2, in agreement with the continuous medium model of H. Spiering.[6,7] In addition, Eq. (14) evidences the direct synergy between the effective "field," $\frac{1}{2}(\Delta - k_B T \ln g)$, which stabilizes the LS (HS) state at low (high) temperatures and the elastic contribution in the local field-like h_i, which does the same. Indeed, the sign of the quantity $-A_0\rho_1 \sum_{j=1}^{z}[(r_{ij} - \rho_0)]$ reverses from positive to negative when the lattice goes from LS ($r_{ij} = R_0^{\mathrm{LL}}$) to HS ($r_{ij} = R_0^{\mathrm{HH}}$) states. Thus, the local field-like h_i constitutes one of the driving forces of the SC transition. An important issue of this model is the direct identification of the effective interaction term J_{ij} with the elastic energy associated with the volume misfit between the HS and the LS lattices. Interestingly, this short-range effective interaction is strictly positive and thus the coupling is antiferroelastic and leads to stabilize energetically the HS-LS configurations at short range. However, the elastic interaction arising from the local field-like contribution, h_i, is long ranged and favors the appearance of HS or LS domains. In a recent work we reported on the coexistence of antiferroelastic and ferroelastic correlation functions, for nearest neighbors and long distance, respectively.[30] A competition between these two contributions may lead to observe self-organized structures, reminiscent of two-step transitions, a work which will be addressed elsewhere.

It is emphasized that the present model including the anharmonic part is not a standard compressible Ising model, in which the displacement field should couple to the squared spin field.[29] The present bilinear coupling is not possible in true magnetic systems because of symmetry breaking by time reversal but is allowed here due to the different symmetry properties of the pseudospins.

The way the total Hamiltonian is solved may be the most crucial issue for the physical relevance of the model, and it involves the different time scales of the spin-state switching and of the lattice dynamics. Representative values of the spin-state lifetimes in the temperature range of the thermal transition typically are in the millisecond range (and far above at lower temperatures). On the other hand, the distortions are expected to propagate at the velocity of sound in the crystal (some 10^3 m/s) and, consequently, propagate through a unit cell (10^{-9} m) within typically less than 1 μs. Therefore, we assumed that after each spin switching the lattice has time enough to (almost) relax the excess elastic energy generated by the spin

switching. Consequently, we used a two-step iterative strategy, as follows: (i) randomly select a given site and perform an eventual spin-state switching according to a Monte Carlo procedure based on the variation of the energy of the system and (ii) perform the site displacements by a Metropolis Monte Carlo update. During steps i and ii the lattice and the spins are frozen, respectively. Step i is similar to a Franck-Condon process; step ii performs a sufficient number of Monte Carlo cycles, typically 1000, to approach mechanical equilibrium.

III. CHOICE OF PARAMETER VALUES

The relationships between electronic parameters and thermodynamic data on the system are well known for Ising-like models (see, e.g., Refs. 11, 13, and 26. The LS-HS energy gap Δ is related to the molar enthalpy variation upon complete transition, according to $\Delta H = N_A \Delta$, where N_A is the Avogadro number. The values of ΔH are in the range 5–20 kJ/mol.[31] The degeneracy ratio is related to the molar entropy change upon complete transition ΔS, according to $\Delta S = R \ln g$, where R is the perfect gas constant. The values of ΔS are in the range 35–80 J/K/mol. In the present work we used $\Delta = 900$ K and $\ln g \simeq 10$, respectively, leading to $\Delta H \approx 7.5$ kJ/mol and $\Delta S \approx 83$ J/K/mol. The corresponding value of the transition temperature is

$$T_{\rm eq} = \frac{\Delta H}{\Delta S} = \frac{\Delta}{k_B \ln g}, \tag{15}$$

which is equal to ≈90 K for the used parameter values. Some of the elastic parameter values of the model can be derived from the known properties of the pure phases (LS or HS). For example, the equilibrium Fe(II)-ligand distances increase by about 10% upon the LS-HS transition,[2] but the variations of the lattice parameters usually are closer to a few percent. We actually used, for the first- neighbor pairs (lattice parameter distance), $R_0^{\rm LL} = 1$ nm, $R_0^{\rm HH} = 1.2$ nm, and for the second-neighbor pairs, $R'^{\rm LL}_0 = \sqrt{2} R_0^{\rm LL}$, $R'^{\rm HH}_0 = \sqrt{2} R_0^{HH}$, based on the idea that the angular distortions[32] may be neglected. The choice of such a large lattice parameter variation is rather arbitrary since the relationship between the lattice parameter and the metal-ligand bond distance variations is certainly complex, and it is so far unknown. In addition, the use of a large value of the lattice mismatch is expected to balance the reduction in stress effects due to the small size of the lattice. Moreover, the possible overestimate of the lattice mismatch parameter can be merely compensated by a decrease in the bulk modulus value, as shown by Eqs. (10) and (13). In other words, we believe that the qualitative nature of the phenomenon is universal.

The values of the harmonic interaction parameters A_{ij} in the HS and LS phases can be derived from the bulk modulus E, which, in SC solids, amounts to ≈5–20 GPa.[33,34] An order of magnitude of the stiffness constant A_0 is obtained by considering the elongation of a cubic cell using a 3D lattice, with lattice parameter a, submitted to an uniaxial stress, and neglecting the transversal effects. This simplified model results in the (approximate) relationship $A_0 + 2B_0 \approx Ea$. Following these observations, we took $A_0 \approx 4000$ K/nm^2 ≈ 4 meV/Å^2, leading to the bulk modulus value, $E = 6$ GPa, which is in good agreement with the experimental literature data.[33]

The ratio A_1/A_0 can be estimated by the Debye temperature ratio [Eq. (5)], and we took $A_1 = 4 \times 10^4$ K/nm^2, leading to $A_1 \rho_1^2 = 100$ K. This simple working assumption concerned terms which apparently did not play a leading role at the transition, and it was not further questioned in the course of the present work.

IV. RESULTS AND ANALYSIS

We investigated here the thermal properties of a planar square system ($50 \times 50 = N = L^2$) with free boundary conditions. The temperature was increased from $T = 0$ to 200 K, then decreased to 0 K, in 1 K increments. As described in Sec. II, the stochastic procedure was alternatively performed on spin and lattice variables, with 1000 lattice Monte Carlo cycles after each eventual spin-state switch. Random application of the two-step Monte Carlo procedure over all sites of the lattice—termed here a "spin-lattice Monte Carlo cycle"—was repeated 2.0×10^3 times at each temperature. The first 10^3 times were used to reach the equilibrium of the system, and the second 10^3 times for the statistical analysis of the physical quantities of interest. We first determined the phase diagram of the thermal transition of the system in order to validate the model (with respect to the well-known properties of SMSs) and in the second step we analyzed the spatiotemporal features of the thermal transition, from both electronic and structural viewpoints.

A. The thermally induced first-order transition and phase diagram

We first investigated the average properties of the system, with the HS fraction defined as

$$n_{\rm HS} = \frac{(1 + \langle S_i \rangle)}{2}, \tag{16}$$

and that of the lattice parameter given by

$$\langle d \rangle = \frac{\sum_{ij} \sqrt{(x_j - x_i)^2 + (y_j - y_i)^2}}{N(N-1)/2}, \tag{17}$$

where i, j run over $[1,N]$ and are restricted to first-neighbor pairs. The simulation results are shown in Fig. 1 for different

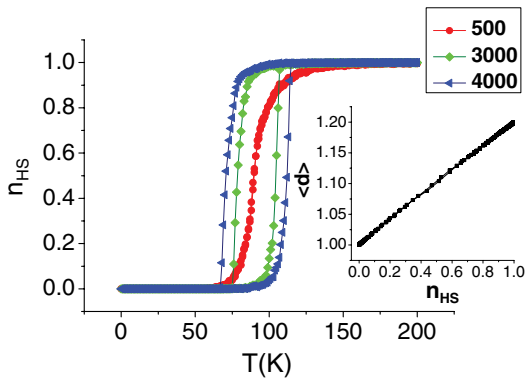

FIG. 1. (Color online) Thermal dependence of the HS fraction for different values of the elastic constant A_0. Inset: Correlation between the lattice parameter $\langle d \rangle$ and the HS fraction (computed for $A_0 = 4000$ K/nm^2).

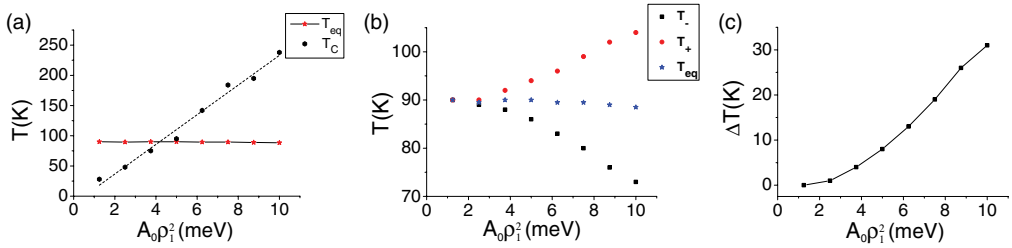

FIG. 2. (Color online) (a) Dependence of T_C and T_{eq} on $A_0\rho_1^2$; (b) phase diagram of the system, where T_+, T_- are the limiting temperatures of the hysteresis loop and T_{eq} is approximated by $\frac{(T_+ + T_-)}{2}$. (c) Dependence of the hysteresis width ΔT on $A_0\rho_1^2$.

values of the harmonic elastic constant A_0 in the range of the significant values determined in the previous section. Upon increasing A_0, the transition transforms from gradual to first-order. A_0 can be scaled to the phenomenological interaction parameter of the usual two-level models through Eq. (13), and we derived a phase diagram in elastic terms, which is shown below. The slightly rounded shape of the simulated hysteresis loop denotes the existence of kinetic effects, previously characterized by the Ising-like model. Also, a clear correlation could be established between the two order parameters, as shown in the inset in Fig. 1.

As shown in Fig. 1, the model exhibits a phase transition due to the elastic interaction, which is now discussed by analogy to the usual phenomenological description.[11,26] For the needs of the coming discussion, we characterized the order-disorder temperature of the system, T_C, as the "critical temperature" resulting from Hamiltonian (9) in the case where the local field-like, h_i, is set to 0. For this specific case, we set $\Delta = 0$, $g = 1$ (non-degenerate states) in the expressions (9) and (11). In other words, we considered a "pure" Ising model with an exchange interaction parameter $A_0\rho_1^2$ on which we performed Monte Carlo simulations and calculated the thermal dependence of the magnetization, $\langle S \rangle$, for determining its order-disorder temperature. A second-order phase transition was then obtained, despite the existence of a negligible residual elastic field contribution in the local field-like h_i [see Eq. (14)]. We have studied the dependence of this order-disorder temperature, T_C, on the elastic energy $A_0\rho_1^2$. The results are reported in Fig. 2(a), where the T_C data (black symbols) are compared to the equilibrium temperature values T_{eq} (for which $n_{HS} = 0.5$; red symbols).

We found that T_C is proportional to $A_0\rho_1^2$,

$$T_C \approx \alpha A_0 \rho_1^2, \tag{18}$$

while T_{eq} does not depend on the elastic interaction parameter A_0. This is mainly due to the fact that the average contribution of the elastic "field," $A_0\rho_1 \sum_1^Z (r_{ij} - \rho_0)$, to the local field-like contribution, h_i [given in Eq. (14)], is negligible, which agrees with Eq. (15). As a general property, the criterion for the existence of a first-order transition is given by $T_{eq} < T_C$. We have plotted the upper, T_+, and lower, T_-, transition temperatures of the hysteresis loop in Fig. 2(b) and the dependence of the hysteresis width, ΔT, on the elastic interaction $A_0\rho_1^2$ in Fig. 2(c). The obtained phase diagram demonstrates, as expected, a critical value of the elastic constant parameter. The borderlines in this diagram are slightly curved at the vicinity of the critical point, and we checked that this effect is due to the finite value of the temperature sweeping rate (kinetic effect). For the data reported in Fig. 2(a), we scanned A_0 while keeping ρ_1 constant. We also checked that T_C was proportional to ρ_1^2 when A_0 was kept constant. This simple dependence of T_C on the mismatch energy was assumed in a recent theoretical work on the effective character of the long-range interaction in the frame of the short-range interacting model.[35]

1. *Lattice configurations upon the SC transition*

Now we report on the elastic properties of the lattice at some positions on the hysteresis loop shown in Fig. 3(a). In Fig. 3(b) we show the corresponding snapshots of the system. In Fig. 3(c) we plot the distribution of the local pressure $P(i)$ defined as

$$P(i) = -\sum_j A_{ij}(r_{ij})(r_{ij} - R_0(S_i, S_j)) - \sum_k B_{ik}(r_{ik})(r_{ik} - R_0(S_i, S_k)), \tag{19}$$

where j (k) runs over nearest (next-nearest) neighbors of site i.

Figure 3(b) gives evidence for a domain growth process starting from all corners, for both the HS $\rightarrow$ LS and the LS $\rightarrow$ HS transformations, as already reported by previous molecular dynamics and Monte Carlo studies.[17,36] The growing domains extend towards the center of the crystal and then collapse. This behavior is reminiscent of experimental observations obtained by optical microscopy,[23] for which the NG process starts from a single point (edge, corner, or defect) and can propagate through the entire crystal under isothermal conditions. However, simultaneous nucleation at all corners followed by propagation toward the center has not been experimentally observed so far. A possible reason for this difference may be a shape effect, because all crystals investigated till now always departed from the perfect square shape of the present model. An alternative explanation might be the (unavoidable) presence of defects in real systems.

The maps of the local pressure, shown in Fig. 3(c), mainly show short-range inhomogeneous distributions of pressures resulting from local expansions and shrinkages. Along the cooling branch (from B to C), the peaks of positive pressure progressively take over, due to the cooperative effect of the local shrinkages resulting from the growth of LS domains, and the reverse is observed (mutatis mutandis) along the heating branch. The onset of such inhomogeneous structures was reported during the domain wall propagation observed by optical microscopy.[23]

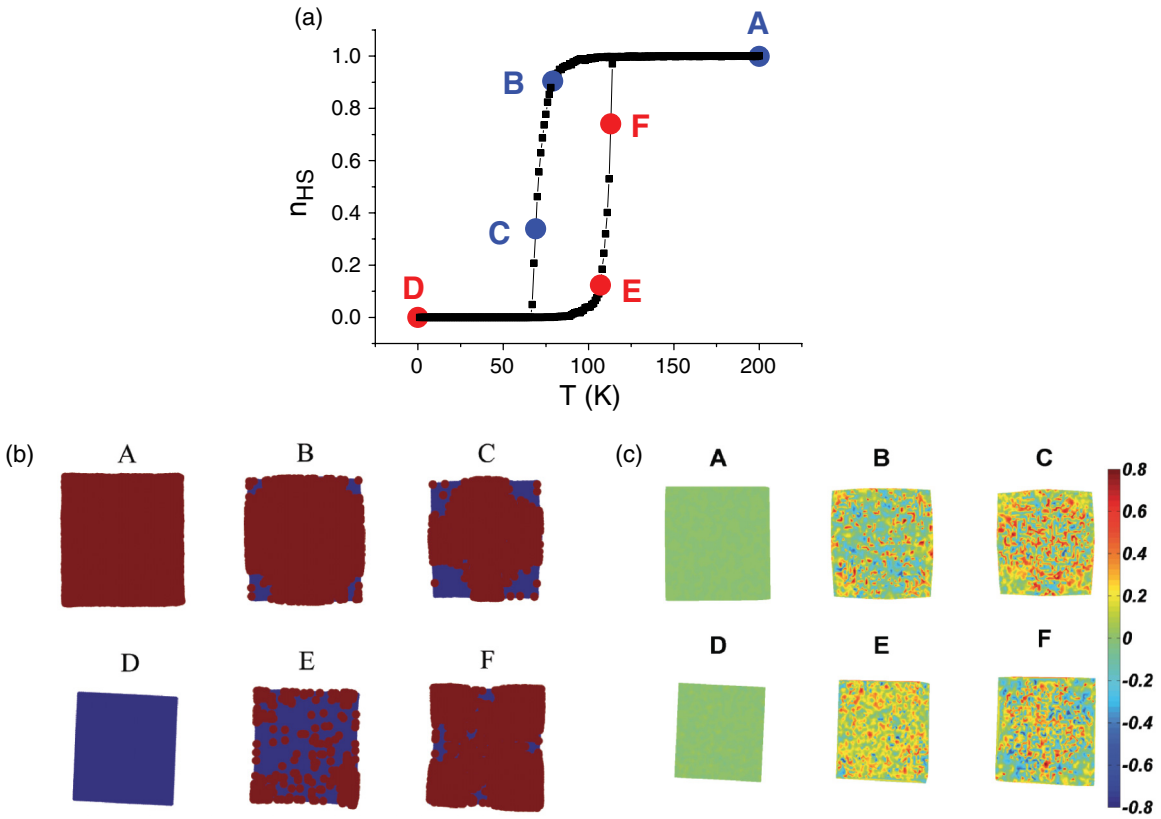

FIG. 3. (Color online) (a) Calculated thermal hysteresis loop for $A_0\rho_1^2 = 160$ K. (b) Snapshots of the system at positions A to F. Red and blue filled circles are associated with HS and LS units, respectively. (c) Snapshots of the local pressure map (defined in text).

We can explain why nucleation in the model starts from the corners, by simple energetic considerations. Let us start from a lattice in a saturated HS state and consider a nucleus made of a single LS site. The energy cost associated with the creation of an LS nucleus at the corner, edge, and center of the HS lattice is written

$$\begin{aligned}\Delta E_{\text{corner}} &= E(\text{LS}) - E(\text{HS}) \\ &= -(\Delta - k_B T \ln g) + 4(A_0 + B_0)\rho_1^2, \end{aligned} \quad (20)$$

$$\Delta E_{\text{edge}} = -(\Delta - k_B T \ln g) + 2(3A_0 + 4B_0)\rho_1^2, \quad (21)$$

$$\Delta E_{\text{center}} = -(\Delta - k_B T \ln g) + 4(2A_0 + 4B_0)\rho_1^2. \quad (22)$$

The first contribution to Eqs. (20)–(22), that is, the temperature-dependent field, is negative due to the situation of the system in the metastable state. The second term is positive, and it is obviously minimized at the corner position. Upon heating, similar considerations can be developed, with the only difference that larger thermal fluctuations may increase slightly the (low) probabilities of nucleation at the center or edges, with respect to the corner position.

In addition, we calculated the total elastic energy of the HS lattice with an LS atom embedded at the corner, at the edge, and in the center. We show in Fig. 4 how the energy relaxes in these cases. Clearly, the elastic energy is best relaxed in the corner case.[17] This should make further growth easier. The relaxation process of the elastic energy is an important issue which will be detailed separately.

B. Analysis of the displacement field

Now we focus on the stresses generated by the NG process, which have been shown to be important in experiments. We determined the elastic stresses at the various positions (A–F) in Fig. 3. To do so, we introduced a displacement field $\vec{u}(i_x,i_y)$ associated with the lattice site (i_x,i_y), defined as

$$\vec{u}(i_x,i_y) = \vec{r}(i_x,i_y) - \vec{r}_0(i_x,i_y), \quad (23)$$

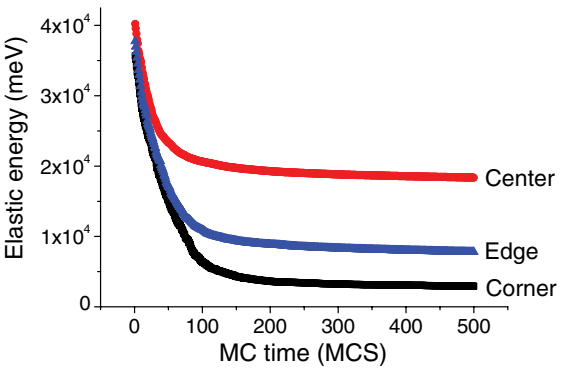

FIG. 4. (Color online) Spontaneous evolution of the elastic energy of an LS lattice through mechanical relaxation when one atom of the lattice has been set in the HS state, in a corner [bottom (black) curve], at an edge [middle (blue) curve], and in the center [top (red) curve]. The time scale is expressed in Monte Carlo steps, and calculation was performed at a low temperature (1 K).

where $\vec{r}_0(i_x,i_y)$ and $\vec{r}(i_x,i_y)$ are the initial and final atomic positions of site (i_x,i_y). In the present analysis, we used the positions in the perfect HS state as a reference state, i.e.,

$$\vec{r}_0(i_x,i_y) = \left(i_x R_0^{\mathrm{HH}}, i_y R_0^{\mathrm{HH}}\right). \tag{24}$$

Deformations are obtained by deriving the displacement expressions: in the continuum approximation,

$$\frac{\partial u_x}{\partial x} = \frac{u_x(i_x+1,i_y) - u_x(i_x,i_y)}{R_0^{\mathrm{HH}}}, \tag{25}$$

and $\frac{\partial u_y}{\partial y}$, $\frac{\partial u_x}{\partial y}$, and $\frac{\partial u_y}{\partial x}$ are also given in the same way. In the case of a harmonic potential, the potential energy is transformed into the continuum elastic potential with a square symmetry according to

$$H_{\mathrm{elas}} = \int d\vec{r}\left\{\frac{A_0+B_0}{2}(\epsilon_{xx}(\vec{r})^2 + \epsilon_{yy}(\vec{r})^2) + B_0\epsilon_{xx}(\vec{r})\epsilon_{yy}(\vec{r}) + 2B_0\epsilon_{xy}(\vec{r})^2\right\}, \tag{26}$$

where $\epsilon_{\alpha\beta}$ represents the strain tensor

$$\epsilon_{\alpha\beta} = \frac{1}{2}\left(\frac{\partial u_\alpha}{\partial x_\beta} + \frac{\partial u_\beta}{\partial x_\alpha}\right) \tag{27}$$

and α, β may be x or y and $x_x = x$, $x_y = x$. It is known that when $A_0 = 2B_0$, the system reduces to an isotropic one with the Lamé coefficients, $\lambda = \mu = B_0$. In the present simulation, we took $A_0 = B_0$ and thus gave the system square symmetry.

We have calculated the displacement field and its spatial distribution at different temperatures at positions A–F along the hysteresis loop in Fig. 3. We derived the spatial distribution of the strain tensors, ϵ_{xx}, ϵ_{yy}, ϵ_{xy}, and ϵ_{yx}. The first two terms ϵ_{xx} and ϵ_{yy} provide information about the local relative volume change and the last two terms ϵ_{xy} and ϵ_{yx} are related to the pure shear strains.

We also derived the following fields, denoted the "dilatation" and "distortion" fields, respectively:

$$\mathrm{div}[\vec{u}(\vec{r})] = \epsilon_{xx}(\vec{r}) + \epsilon_{yy}(\vec{r}) \quad \text{and}$$
$$\vec{\mathrm{rot}}[\vec{u}(\vec{r})] = \epsilon_{xy}(\vec{r}) - \epsilon_{yx}(\vec{r}). \tag{28}$$

The divergence of the displacement field, that is, the trace of the strain tensor, describes the pure relative volume (here surface) expansion.

We have mapped the dilation and distortion fields, in Figs. 5 and 6, respectively, at positions A $\leftrightarrow$ F along the hysteresis loop defined in Fig. 3. An obvious correlation between the dilatation maps in Fig. 5 and the spin configurations in Fig. 3 is observed. However, the dilatation maps of the cooling and the heating branches clearly differ. Due to the choice of the HS state as the reference state, the divergence of the displacement field starts from 0 in the HS state [Fig. 5(a)] and becomes negative in the cooling mode, corresponding to the shrinking of the system. The detailed observation of the distortion maps at positions B and C shows that the shrinking is mainly concentrated at the corners of the lattice, while it is weak at the center and on the edges. This feature is associated with a nucleation process starting from the corners. Upon heating (positions E and F), similar observations can be made (for an expansion effect).

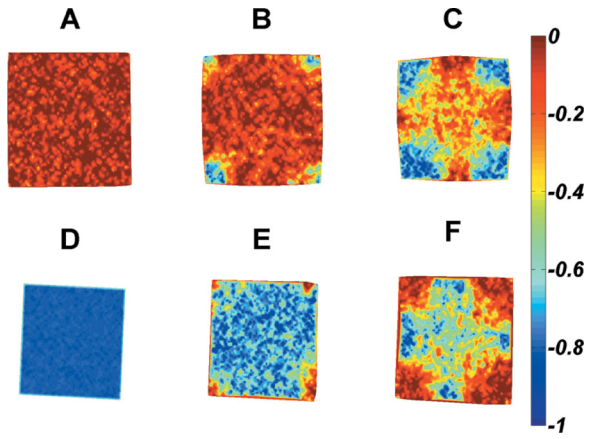

FIG. 5. (Color online) Maps of the divergence of the displacement field at different positions along the hysteresis loop in Fig. 3. The reference state is the HS phase, thus leading to a negative value of the divergence, which reaches its maximum value in the saturated LS state.

The distortion field gives evidence for an enhancement of the shear stresses at the intersects of the transformation frontline and the edges of the lattice. These regions constitute brittle points at which dislocations and/or fractures may be initiated. The understanding of these aspects is of major importance for technological applications of the SMSs. The quantity $e = \epsilon_{xx} - \epsilon_{yy}$ describes deviatoric shear strains[37] but is not analyzed here. It plays an important role in the onset of fractures in the material, an interesting problem which will be treated separately.

V. THE ELASTIC LONG-RANGE NATURE OF THE INTERACTION BETWEEN SC ATOMS AND THE FORMATION OF SPIN DOMAINS

It is well known that elastic effects generate long-range interactions. For example, a classical behavior was observed in the gas-liquid transition of hydrogen in metals,[38] in structural phase transitions,[39] and in ferroelectrics[40] long ago. The

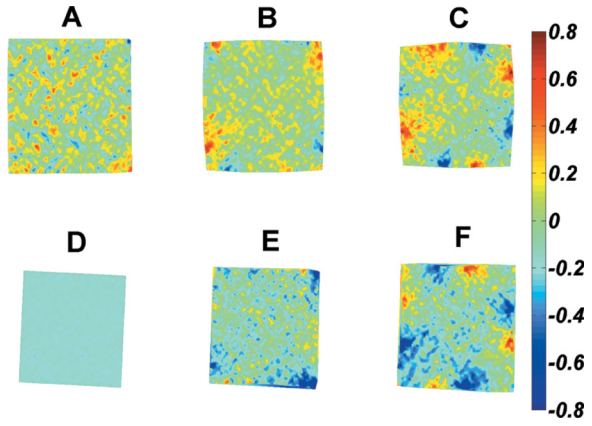

FIG. 6. (Color online) Maps of the rotation of the displacement field at several positions along the hysteresis loop in Fig. 3. The maximum values are observed at the edges of the system and/or at the interfaces between the LS and the HS domains, as depicted in images B, C, E, and F. They outline the presence of shear strains.

theoretical side of the problem was considered in Ref. 41, and other pioneering works.[42] It is also quite well established that an elastic interaction between dipolar elastic defects[41] (i.e., localized stresses) decays as r_{ij}^{-3}. However, the defect-defect interaction is strongly modified by the shape of the lattice and by finite-size effects.[43] The long-range character of the present model plays an important role in the domain formation and also in the deformation of the lattice edges reported in Fig. 3. It has been discussed in the pure elastic model proposed in Ref. 15, which has been shown to belong to the mean-field universality class. In addition, recent investigations on circularly shaped lattices have evidenced the macroscopic character of the NG phenomena involved in this class of models,[21] as well as the importance of shape effects.

However, the literature on elastic models devoted to the SC problem does not contain any explicit formulation of the long-range character of the interaction. To quantify the long-range character of the present elastic model, we have investigated some typical situations obtained by inserting one and two defects in a homogeneous lattice. We started with a lattice in the LS state (for both electronic and structural degrees of freedom) and then we flipped only one spin (from the LS to the HS state) located at the center of the lattice (far from the borders), and then we performed Monte Carlo and/or molecular dynamics simulations including a friction term in order to reach the mechanical equilibrium in a frozen spin configuration. We then made a quantitative analysis of the computed displacement field $\vec{u}(i_x,i_y)$.

1. *The case of a single point defect*

We consider here the spatial dependence of the displacement field around an HS atom embedded in an LS lattice. We have drawn the two components u_x and u_y of the atomic displacements of the neighboring atoms of the defect at position (i_{x0},i_{y0}) in the x and y directions as a function of their distance $d(i_x,i_y) \equiv \sqrt{(i_x - i_{x0})^2 + (i_y - i_{y0})^2}$ from the HS defect. As shown in Fig. 7(a), due to the symmetry of the lattice and shape of the defect (here a point-like defect), the components u_x and u_y are strictly equal (save for numerical errors). The deformation field caused by the perturbed atom visibly propagates at least up to the ≈10th neighbor, thus evidencing the long-range character of the effective interaction.

We have reported in Fig. 7(b), the spatial evolution of the absolute value of the displacement, i.e., $u_x(i_x,i_y)$ as a function of $1/d(i_x,0)$. The results clearly show that the displacement field follows the law

$$u_x = \frac{m}{d(i_x,0)} + U_\infty, \tag{29}$$

where the fitted parameter values are $m = 0.04623(2)$ nm^2 and $U_\infty = -0.0043(6)$ nm. The constant U_∞ can be understood as the effect of the image pressure resulting from the finite shape of the system and vanishes at the limit of large systems. We have checked that an identical radial dependence was obtained in any direction around the defect site. This property gives to the displacement field in an infinite system the simple radial dependence $u \propto \frac{m}{r}$. The specific dependence of this displacement field obeys the Gauss theorem, and we expect

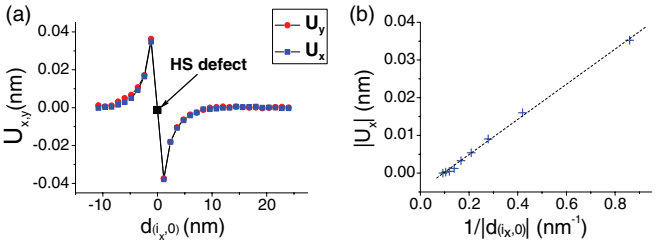

FIG. 7. (Color online) (a) Atomic displacements (u_x and u_y) of neighboring atoms of the HS defect at position (i_{x0},i_{y0}) in the x and y directions versus their distance $d(i_x,i_y) \equiv \sqrt{(i_x - i_{x0})^2 + (i_y - i_{y0})^2}$ from the defect. Because of the square symmetry, we have $u_y = u_x$. (b) Linear fitting of the displacement of the atoms in the x direction versus the inverse of the distance $1/d(i_x,0)$ showing that $u_x(i_x,i_y) \propto 1/d(i_x,0)$. The slope is proportional to the lattice misfit (see text for more explanations). The parameter values are the same as those in previous figures.

the same property in 3D systems, then leading to the r^{-2} radial dependence of the displacement field. We have checked that different values of the elastic constants A_0 and A_1 led to similar results, and this indicated that the obtained behavior is universal and makes possible a tight analogy with the properties of elastic continuous media.

We carefully investigated the dependence of the slope m of this universal curve on the lattice mismatch associated with the nature of the defect. We separately considered various values of $(R_0^{\mathrm{HH}} - R_0^{\mathrm{HL}})$ at constant $(R_0^{\mathrm{HH}} + R_0^{\mathrm{HL}})$, and vice versa. We observed that the slope m was proportional to both of these factors, and consequently, it was merely expressed as

$$m \propto \left[\left(R_0^{\mathrm{HH}}\right)^2 - \left(R_0^{\mathrm{HL}}\right)^2\right] \approx a\rho_1. \tag{30}$$

Similar displacement fields, following $u \propto 1/r^{d-1}$, are obtained in the frame of linear elasticity theory for radially symmetric strain around any point-like perturbation in a $d = 2$ or $d = 3$ medium. The remarkable finding of the present model is that Eq. (30) yields also the amplitude of this strain if it is caused by an embedded LS or HS atom inside an HS or LS lattice, respectively. The amplitude of the displacement field is directly related to the lattice misfit, ρ_1, while the specific form of the interaction potential drops out from the results. The displacement field within this model is then a topological property of the point-like defect.

2. *The case of two point defects: Elastic interaction energy*

Tor elucidate the nature of the elastic interaction between SC units, we considered the case of two HS point defects embedded in an LS lattice. We calculated the elastic energy of the ground state of the system as a function of the interdefect distance, denoted r. The obtained results are reported in Fig. 8(a), and they clearly show that the two defects are submitted to an attractive interaction. A simple quantitative analysis of the data [see inset in Fig. 8(a)] demonstrates that the elastic energy follows the simple law

$$E_{\mathrm{elas}} = c - \frac{\alpha}{r^2}, \tag{31}$$

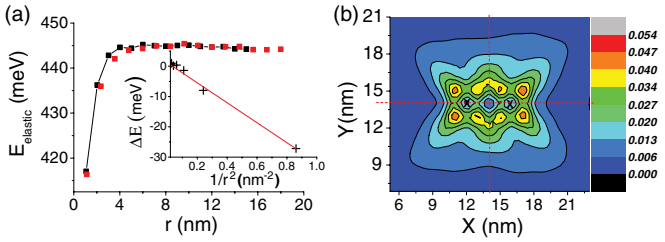

FIG. 8. (Color online) (a) Evolution of the total elastic energy in the case of two HS atoms embedded in an LS lattice, as a function of their distance. The attractive interaction between the defects is inferred from the decrease in the elastic energy at short distances. Inset: This plot of $E(r) - E(r \longrightarrow \infty)$ versus $1/r^2$ characterizes the radial dependence of the interaction. (b) Spatial distribution of the atomic displacement field (the LS state is the reference state); defects are indicated by (black) crosses. The specific shape of the contour plots demonstrates the attractive character of the deformation field in the space between the two defects and its repulsive nature far away. Lattice size was 20×20.

where c ($\approx$445 meV) is the elastic energy generated by two independent defects located far away from each other, and α is a constant proportional to the misfit parameter between the LS and the HS lattices.

We also considered the reverse situation, that is, the case of two LS defects embedded in an HS lattice, which led to similar results [shown as light (red) squares in Fig. 8(a)]. This means that the elastic energy does not depend on the sign of the misfit parameter, in agreement with the conclusions drawn for the one-point defect.

Equation (31) expresses the interaction between the strain fields, $\epsilon_1(r)$ and $\epsilon_2(r)$, produced by two defects considered independently. The overlap of these strain fields gives rise to an interaction energy $\simeq \epsilon_1(r)\epsilon_2(r)$, which vanishes in an infinite medium.[44] One can understand this by noting that $\epsilon_1(r)$ and $\epsilon_2(r)$ have opposite signs (i.e., the interaction is attractive) in the space between the two centrers, but far away from the defects they have the same sign as depicted in Fig. 8(b).

In a finite system bounded by a surface [i.e., when the system size has the same order of magnitude as the distance between the defects; see Fig. 8(b)], the situation may be sizably different: the deformation field stops at the surface and this favors the attractive character of the interaction energy. These surface effects will be analyzed in detail in a forthcoming report, in which we address the case of a finite system containing a distribution of dilatation centers.

VI. CONCLUSION

We have presented a deformable-lattice SC model with realistic parameter values, aiming to reproduce the spatiotemporal behavior of SC solids. The model contains both spin and lattice degrees of freedom and allows a complete description of the thermal behavior of the SMSs. We have demonstrated that this model can be mapped under the form of an Ising-like model with effective interaction parameters depending on the lattice parameter misfit between the LS and the HS phases and on the bulk modulus of the material. This mapping allowed us to establish the phase diagram of the model, from which the gradual and the first-order transitions as well as the transition temperature were analytically predicted. We also studied the thermal dependence of the lattice configurations upon cooling and heating along the thermal hysteresis loop and characterized the evolution of the system at a constant temperature when it is prepared in a metastable state. We have introduced, for the first time in this type of model, the calculation of the local strains, displacements, and deformation fields, which govern the transition mechanism. The results agree with expectations derived from experimental observations by optical microscopy. Although not investigated in this work, the relaxation properties of the photoinduced metastable state can be accessed as well through the present model.

Ongoing developments of the simulations should include the effect of a bilinear interaction, given in Eq. (7), by considering the case $R_0^{\mathrm{HL}} \neq \frac{R_0^{\mathrm{HH}} + R_0^{\mathrm{LL}}}{2}$. The present model has the advantage of producing naturally short-range and long-range interactions. The sign of these interactions might be reversed according to the parameter values, which is expected to lead to a simple description of the two-step SC behavior, which so far is restricted to the phenomenological level.

ACKNOWLEDGMENTS

The present work was supported by the University of Versailles, where the results were obtained. Acknowledgments are also due to the Centre National de la Recherche Scientifique (CNRS), Groupement de Recherche International (GDRI) France-Japan, and Pôle de Recherche et d'Enseignement Supérieur (PRES-UniverSUd) for the Commutation aux Petites Echelles Spatiales (COPECS) project and to a Grant-in-Aid for Scientific Research C (No. 23540381) from MEXT of Japan.

*Corresponding author: kbo@physique.uvsq.fr

[1] E. König, Struct. Bonding **76**, 51 (1991).
[2] P. Gütlich, A. Hauser, and H. Spiering, Angew. Chem. Int. Ed. Engl. **33**, 2024 (1994).
[3] S. Decurtins, P. Gütlich, C. P. Köhler, H. Spiering, and A. Hauser, Chem. Phys. Lett. **105**, 1 (1984).
[4] G. D'Avino, A. Painelli, and K. Boukheddaden, Phys. Rev. B **84**, 104119 (2011).
[5] N. Willenbacher and H. Spiering, J. Phys. C **21**, 1423 (1988).
[6] H. Spiering and N. Willenbacher, J. Phys.: Condens. Matter **1**, 10089 (1989).
[7] H. Spiering, Top. Curr. Chem. **235**, 171 (2004).
[8] C. P. Köhler, R. Jakobi, E. Meissner, L. Wiehl, and H. Spiering, J. Phys. Chem. Solids **51**, 239 (1990).
[9] R. Jakobi, H. Spiering, and P. Gütlich, J. Phys. Chem. Solids **53**, 267 (1992).
[10] K. Boukheddaden, J. Linares, E. Codjovi, and F. Varret, J. Appl. Phys. **93**, 7103 (2003).
[11] A. Bousseksou, J. Nasser, J. Linares, K. Boukheddaden, and F. Varret, J. Phys. I France **2**, 1381 (1992).
[12] C. P. Slichter and H. G. Drickamer, Chem. Phys. **56**, 2142 (1972).
[13] J. Wajnflasz and R. Pick, J. Phys. (Paris) Colloq. **32**, C1 (1971).

[14]S. Doniach, J. Chem. Phys. **68**, 4912 (1978).
[15]S. Miyashita, Y. Konishi, M. Nishino, H. Tokoro, and P. A. Rikvold, Phys. Rev. B **77**, 014105 (2008).
[16]M. Nishino, K. Boukheddaden, Y. Konishi, and S. Miyashita, Phys. Rev. Lett. **98**, 247203 (2007).
[17]M. Nishino, C. Enachescu, S. Miyashita, K. Boukheddaden, and F. Varret, Phys. Rev. B **82**, 020409(R) (2010).
[18]L. Stoleriu, P. Chakraborty, A. Hauser, A. Stancu, and C. Enachescu, Phys. Rev. B **84**, 134102 (2011).
[19]C. Enachescu, L. Stoleriu, A. Stancu, and A. Hauser, Phys. Rev. Lett. **102**, 257204 (2009).
[20]W. Nicolazzi and S. Pillet, Phys. Rev. B **85**, 094101 (2012).
[21]M. Nishino, C. Enachescu, S. Miyashita, P. A. Rikvold, K. Boukheddaden, and F. Varret, Sci Rep. Nature PG **1**, 162 (2011).
[22]F. Varret, A. Slimani, K. Boukheddaden, C. Chong, H. Mishra, E. Collet, J. Haasnoot, and S. Pillet, New J. Chem. **35**, 2333 (2011).
[23]A. Slimani, F. Varret, K. Boukheddaden, C. Chong, H. Mishra, J. Haasnoot, and S. Pillet, Phys. Rev. B **84**, 094442 (2011).
[24]C. Chong, A. Slimani, F. Varret, K. Boukheddaden, E. Collet, J. C. Ameline, R. Bronisz, and A. Hauser, Chem. Phys. Lett. **504**, 29 (2011).
[25]K. Boukheddaden, M. Nishino, and S. Miyashita, Phys. Rev. Lett. **100**, 177206 (2008).
[26]K. Boukheddaden, I. Shteto, B. Hoo, and F. Varret, Phys. Rev. B **62**, 14796 (2000); **62**, 14806 (2000).
[27]S. Miyashita, Y. Konishi, H. Tokoro, M. Nishino, K. Boukheddaden, and F. Varret, Prog. Theor. Phys. **114**, 4 (2005).
[28]K. Boukheddaden, Pog. Theor. Phys. **112**, 205 (2004).
[29]D. J. Bergman and B. Halperin, Phys. Rev. B **13**, 2145 (1976).
[30]T. Nakada, P. A. Rikvold, T. Mori, M. Nishino, and S. Miyashita, Phys. Rev. B **84**, 054433 (2011).
[31]M. Sorai, Top. Curr. Chem. **235**, 153 (2004).
[32]B. Gallois, J.-A. Real, C. Hauw, and J. Zarembowitch, Inorg. Chem. **29**, 1152 (1990).
[33]J. Jung, F. Bruchhäuser, R. Feile, H. Spiering, and P. Gütlich, Z. Phys. B **100**, 517 (1996).
[34]H. Spiering, K. Boukheddaden, J. Linares, and F. Varret, Phys. Rev. B **70**, 184106 (2004).
[35]T. Nakada, T. Mori, S. Miyashita, M. Nishino, S. Todo, W. Nicolazzi, and P. A. Rikvold, Phys. Rev. B **85**, 054408 (2012).
[36]C. Enachescu, M. Nishino, S. Miyashita, A. Hauser, A. Stancu, and L. Stoleriu, Eur. Phys. Lett. **91**, 27003 (2010).
[37]K. Frankzrahe, P. Nielaba, and S. Sengupta, Phys. Rev. E **82**, 016112 (2010).
[38]H. Wagner, Adv. Phys. **23**, 587 (1974).
[39]R. A. Cowley, Phys. Rev. B **13**, 4877 (1976).
[40]E. Courtens, R. Gammon, and S. Alexander, Phys. Rev. Lett. **43**, 1026 (1979).
[41]H. Wagner and J. Swift, Z. Phys. **239**, 182 (1970).
[42]H. Wagner, Phys. Rev. Lett. **25**, 31 (1970); **25**, 261(E) (1970).
[43]E. R. Grannan, M. Randeria, and J. P. Sethna, Phys. Rev. B **41**, 7784 (1990).
[44]J. D. Eshelby, Sol. Stat. Phys. **3**, 79 (1956).